Progress In Electromagnetics Research, PIER 99, 1–20, 2009

COMPARISON OF PLANAR AND CIRCULAR ANTENNA CONFIGURATIONS FOR BREAST CANCER DETECTION USING MICROWAVE IMAGING

R. C. Conceição, M. O'Halloran, M. Glavin, and E. Jones

Electronic and Electrical Engineering
National University of Ireland Galway
Ireland

Abstract—Ultra Wideband (UWB) radar is a promising emerging technology for breast cancer detection based on the dielectric contrast between normal and tumor tissues at microwave frequencies. One of the most important considerations in developing a UWB imaging system is the configuration of the antenna array. Two specific configurations are currently under investigation, planar and circular. The planar configuration involves placing a conformal array of antennas on the naturally flattened breast with the patient lying in the supine position. Conversely, the circular configuration involves the patient lying in the prone position, with the breast surrounded by a circular array of antennas. In order to effectively test the two antenna configurations, two 2D Finite-Difference Time-Domain (FDTD) models of the breast are created, and are used to simulate backscattered signals generated when the breast is illuminated by UWB pulses. The backscattered signals recorded from each antenna configuration are passed through a UWB beamformer and images of the backscattered energy are created. The performance of each imaging approach is evaluated by both quantitative methods and visual inspection, for a number of test conditions. System performance as a function of number of antennas, variation in tissue properties, and tumor location are examined.

1. INTRODUCTION

Breast cancer accounts for 26% of all female patients suffering from cancer in the United States, where each year, approximately 182,000 cases are diagnosed and approximately 22% of these cases result in

Corresponding author: R. C. Conceição (rqlcdc@gmail.com).

death [1]. The key factors in improving survival rates and quality of life of cancer patients are: reliable diagnosis for early detection, early intervention and reliable monitoring. X-Ray Mammography is currently the *defacto* screening method for detecting non-palpable early breast tumors. However, X-Ray Mammography uses ionising radiation and requires the uncomfortable compression of the breast. Furthermore, the inherent limitations of X-Rays in terms of sensitivity and specificity are well recognised [2].

The false-positive rate associated with X-Ray Mammography can be as high as 75%, causing unnecessary distress to the patient and putting an unnecessary financial burden on the health system. Much more worrying is the false-negative rate of 34%, which reflects situations in which patients are incorrectly diagnosed as not having breast cancer. False-negative results can significantly delay treatment, often to the point where it is no longer effective [3, 4]. These considerable limitations of X-Ray Mammography prompt the development of alternate imaging modalities

In this context, Microwave Imaging is an appealing alternative to X-Ray Mammography as a primary breast cancer diagnosis method. The technology is based on dielectric differences between normal and tumor tissues of the breast at microwave frequencies [5, 6]. There are three different approaches that have been proposed in order to image the breast based on these contrasting dielectric properties: Microwave Tomography, Time-Reversal FDTD methods and UWB Radar Imaging.

The first approach involves a full reconstruction of the dielectric profile of the breast by means of the solution of a forward and inverse scattering problem which seeks to minimise the difference between measured and calculated electric fields [7–12]. Meaney *et al.* [8, 9, 12] have conducted some clinical trials with a tomography prototype system which has produced some promising results. One potential downside of this approach is that inverse scattering problems can potentially have a large computational cost. The Time-Reversal algorithm is based on time-reversing the Finite Difference Time Domain (FDTD) equations, and implies that if a point source radiates and the time-reversed FDTD equations are applied to all points of the grid, the wave will converge back to the source at the time corresponding to the maximum of the initial excitation [13, 14]. Finally, UWB Radar Imaging involves illuminating the breast with a UWB pulse, recording the backscattered signals, and using these signals to identify the presence and location of significant dielectric scatterers within the breast [6, 15–26]. The advantages of UWB radar over traditional X-Ray Mammography include the following:

- It uses non-ionising radiation.
- It offers good resolution capabilities.
- It avoids the uncomfortable compression of the breast associated with X-Ray Mammography.
- It is potentially low cost.

UWB imaging of the breast is based on the dielectric contrast between normal and cancerous tissues at microwave frequencies, and these properties have been the subject of many studies, both historical and recent [8, 27–32]. Malignant tumors present higher values for conductivity and permittivity due to higher concentrations of water, which is caused by abnormal vascularisation [5, 33] and bound water [34, 35]. However, it was recently found that dielectric contrast between fibroglandular and malignant tissue is smaller than previously thought [31, 32], thereby presenting a more challenging imaging scenario. Hence, choosing optimal parameters for UWB breast imaging systems is becoming an increasingly significant problem.

This paper investigates the optimisation of one important aspect of UWB system design for breast cancer imaging, namely, the antenna configuration. The paper is organised as follows: Section 2 reviews the dielectric properties of normal and malignant breast tissue; Section 3 consists of several subsections as follows: the antenna configurations considered, the FDTD model of the breast, the experiments performed, and the metrics used to evaluate the results; Section 4 presents and discusses the experimental results; finally Section 5 draws conclusions from these results.

2. DIELECTRIC PROPERTIES

The dielectric properties of breast tissue (conductivity and permittivity), determine the attenuation, phase, reflection and transmission of UWB signals through the breast. These dielectric properties are briefly reviewed here.

Chaudhary *et al.* [36] examined *ex vivo* specimens of breast tissue removed during cancer surgeries. A significant dielectric contrast between normal and malignant tissues was found across the frequency range of 3 MHz to 3 GHz (contrast ratio of 4.7 : 1 for conductivity and 5 : 1 for relative permittivity). Similar studies which acknowledge the dielectric differences between normal and malignant breast tissue with *ex vivo* experiments include those of Joines [27], who found a contrast ratio of 3.8 : 1 for conductivity and 6.4 : 1 for relative permittivity, and Campbell and Land [30], who found a greater variance of dielectric properties in normal breast tissue compared to previous studies, with relative permittivity varying between 9.8 and 46 and conductivity between 3.7 and 34 mScm^{-1}.

Later, Surowiec *et al.* [29] measured the relative permittivity of infiltrating breast carcinoma and the surrounding tissue. The study found that the tissue at the infiltrating edge of the tumor had increased dielectric properties, suggesting that even quite small tumors could still induce significant microwave backscattering.

Meaney *et al.* [8] performed the first *in vivo* examinations of the dielectric properties of breast tissue using a prototype microwave imaging system. Results showed that the average relative permittivity value at 900 MHz for normal breast tissue was significantly higher than previously published (breasts with higher adipose-fat-tissue content had an average relative permittivity of 31 and heterogeneous dense breasts had an average relative permittivity between 35 and 36).

More recently, Lazebnik *et al.* completed one of the most comprehensive studies to date on dielectric properties of the breast [31, 32]. The dielectric properties of both normal and cancerous breast tissue were analysed and compared. The main findings of Lazebnik's studies included the following:

(i) Adipose tissue has much lower dielectric properties than previously assumed.
(ii) Conversely, fibroglandular tissue has much higher dielectric properties than previously thought.
(iii) The dielectric heterogeneity of normal breast tissue was previously significantly underestimated.

The effect of this dielectric heterogeneity is very significant, and prompts the development of more robust UWB imaging systems.

3. NUMERICAL SIMULATION AND EVALUATION PROCEDURES

In this section, the procedure used to optimise the antenna configuration is detailed. The main steps can be summarised as follows:

- Antenna array configuration
- Numerical breast model
- UWB beamformer
- Test procedure
- Performance metrics

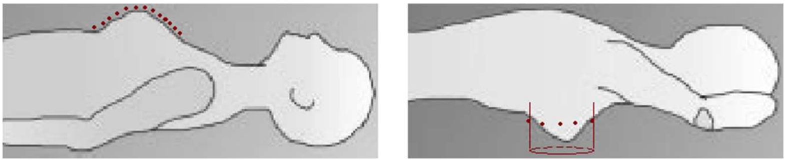

(a) (b)

Figure 1. The supine patient position is shown in (a), while the prone patient position is shown in (b). This image is adapted from [16].

Table 1. Debye parameters for the FDTD model and dielectric properties of each tissue at the centre frequency of the input pulse. The Debye equation is defined as follows: $\epsilon_r^*(\omega) = \epsilon_r + \frac{\sigma}{j\omega\epsilon_0} + \frac{\chi_1}{1+j\omega t_0}$.

Tissue	ϵ_r	χ_1	σ	t_0 (ps)	Relative Perm.	Cond. (S/m)
Skin	15.63	8.2	0.82	12.6	21.65	2.35
Tumor	7	47	0.15	7	49.2	6.1
Adipose	3.20	1.65	0.035	16	4.30	0.38

3.1. Antenna Array Configuration

Two different imaging configurations have been considered: the planar configuration developed initially by Hagness *et al.* [6] and the circular configuration developed by Fear *et al.* [16]. Each configuration is defined by the orientation of the patient and the position of the antenna array. In the planar configuration, the patient is oriented in the supine position with a planar antenna array placed across the naturally flattened breast. This configuration has been used by Hagness, Bond, Davis, Nilavalan, Li and O'Halloran *et al.* [6, 20, 25, 26, 37, 38]. Conversely, in the circular configuration, the patient lies in the prone position with the breast naturally extending through an opening in the examination table. A circular array of antennas surrounds the breast. The circular configuration has been used by Fear, Xie and Klemm *et al.* [18, 39–45]. Both supine and prone positions are shown in Figure 1. In the present study, both configurations of antennas are simulated and compared, extending a previous study [46].

3.2. Numerical Breast Model

In order to test both antenna configurations, a numerical model of the breast is created for both configurations. A 2D FDTD model of the breast, similar to the model used by Hagness *et al.* [6] is used to examine the planar configuration, while a separate circular breast model, as used by Fear *et al.* [39], is also used. In both models, a 2 mm layer of skin covers the breast. The dielectric properties of normal tissue used in [6, 20, 39] are used for the study. In order to account for the dielectric differences between fibrogandular and adipose tissues, there is a dielectric variation of $\pm 10\%$ randomly assigned (using a Gaussian distribution) to 4-mm-side squares within the breast, as used in [6, 39]. Models using dielectric variations of ± 20; ± 30; ± 40 and $\pm 50\%$ were also created.

A Debye model was used to model the frequency-dependent propagation characteristics of the various tissues. The Debye parameters for skin are chosen to fit published data by Gabriel *et al.* [47], while the Debye parameters for malignant tissue are those used by Bond *et al.* [26]. The Debye parameters for each type of tissue, along with the permittivity and conductivity at the centre frequency, are shown in Table 1. For the supine (planar) examination, the breast is naturally flattened and the antennas lie directly on the skin across a span of 80 mm. As the breast flattens, it is assumed that the maximum depth of the breast tissue is 42 mm [6]. The antenna array is backed by a synthetic material matching the dielectric properties of skin. The antenna array elements are modeled as electric-current sources. For the prone (circular) configuration, the antennas form a circle around the breast. The radius of the breast is 36 mm, including the layer of skin [39]. The breast and antenna array are once again backed by a synthetic material matching the dielectric properties of skin. Both models are shown in Figure 2.

The FDTD grid resolution, dx, is 0.5 mm and the time step dt is defined as 0.833 ps ($dt = \frac{dx}{2c}$). A scan involves sequentially illuminating the breast model with a UWB pulse from each antenna, while recording the backscattered signal at the same antenna. Before further processing, the signals are downsampled from 1200 GHz (the time step in the FDTD simulation) to 50 GHz. The input signal is a 150-ps differentiated Gaussian pulse, with a centre frequency of 7.5 GHz and a -3 dB bandwidth of 9 GHz. An idealized artifact removal algorithm is used to remove the input signal and the reflection from the skin-breast interface. The artifact to be removed is established by measuring the backscattered signals from the first homogeneous FDTD model with no tumor present. These signals are then subtracted channel-by-channel from the with-tumor responses. Finally, a delay and sum beamformer is used to create the image of the breast [6, 15–21].

3.3. Test Procedure

Identical simulations are completed for the planar and circular configurations. The performance of each configuration is tested using a varying number of transmitting/receiving antennas. Three tumor positions within the breast are considered, and the tumor itself is 6 mm in diameter. For the circular configuration the tumors are placed at the following (depth, span) locations: the centre of the breast at (−3.6, 3.6) cm, (−3.95, 4.1) cm and (−4.3, 4.6) cm. For the planar configuration the tumor is placed at the following (depth, span) locations: the centre of the breast at (−2.4, 5) cm, (−2.4,3) cm and (−2.4, 1) cm. For clarity of notation, the first location of the tumor is considered to be at a distance 0 from the centre of the breast, the second location at a distance d from the centre of the breast and the third location at a distance $2d$ from the centre of the breast, respectively, in which d represents approximately 0.61 cm for the circular configuration and 2 cm for the planar configuration.

The number of antennas for both configurations is varied between 8 and 20, in steps of 1. Therefore, 39 FDTD simulations are completed for each antenna configuration. The reflected signals are recorded for 5 variations of permittivity and conductivity around their mean value: ±10 to ±50%, in steps of 10%. Therefore, overall 390 individual FDTD simulations were performed.

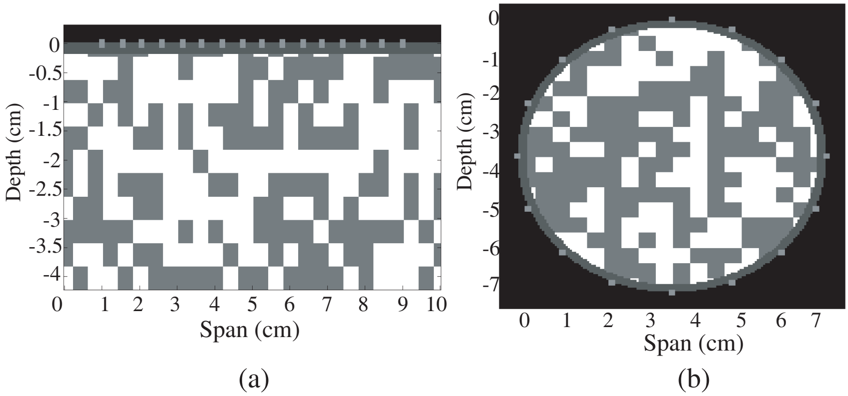

Figure 2. The supine (a), and prone (b), breast models. The lighter regions represent adipose tissue, while the darker regions represent fibroglandular tissue. A 2 mm layer of skin surrounds both models (shown in grey) and the antenna locations are shown in white.

3.4. Metrics

In order to evaluate the robustness and performance of each configuration, a number of different metrics are used:

- Signal-to-Clutter Ratio within-breast (SCR) [16, 42, 46].
- Signal-to-Mean Ratio (SMR) [48].
- The difference between the actual location of the tumor and the location of the peak in the resulting image of backscattered energy (M_{diff}) [38, 46].
- The Full Width Half Maximum (FWHM), which estimates the physical extent of the tumor response [16, 42, 46].

The SCR within-breast compares the maximum tumor response to the maximum clutter response in the same image. To obtain the value of the maximum clutter, the maximum pixel value of the image is found, excluding the area which includes the tumor peak response up to twice the extent of the FWHM response of the tumor itself [16, 42, 46]. The SMR compares the maximum tumor response with the mean response of the different tissues across the breast in the same image of backscattered energy [48]. The FWHM measures the distance between the peak response of the tumor and the point at which the energy of the peak response drops to half [16, 42, 46]. This metric, as well as M_{diff}, determines the ability of the beamformer to effectively localise the tumor within the breast.

The primary aspects of the system performance to be evaluated are:

- The effect of the number of antennas on performance, and the optimal number of antennas required for each antenna configuration.
- The effect of dielectric heterogeneity on system performance.
- The relative performance of the two configurations.

4. RESULTS AND DISCUSSION

4.1. Antenna-number Optimisation

The first experiment involves the number of transmitting/receiving antennas that should be used for optimised performance. Results (SCR and SMR) for both configurations are shown in Figures 3 and 4.

Both the SCR and SMR improve with increasing numbers of antennas for both configurations, with the exception of the planar configuration for the tumor at a distance of $2d$ from the centre of

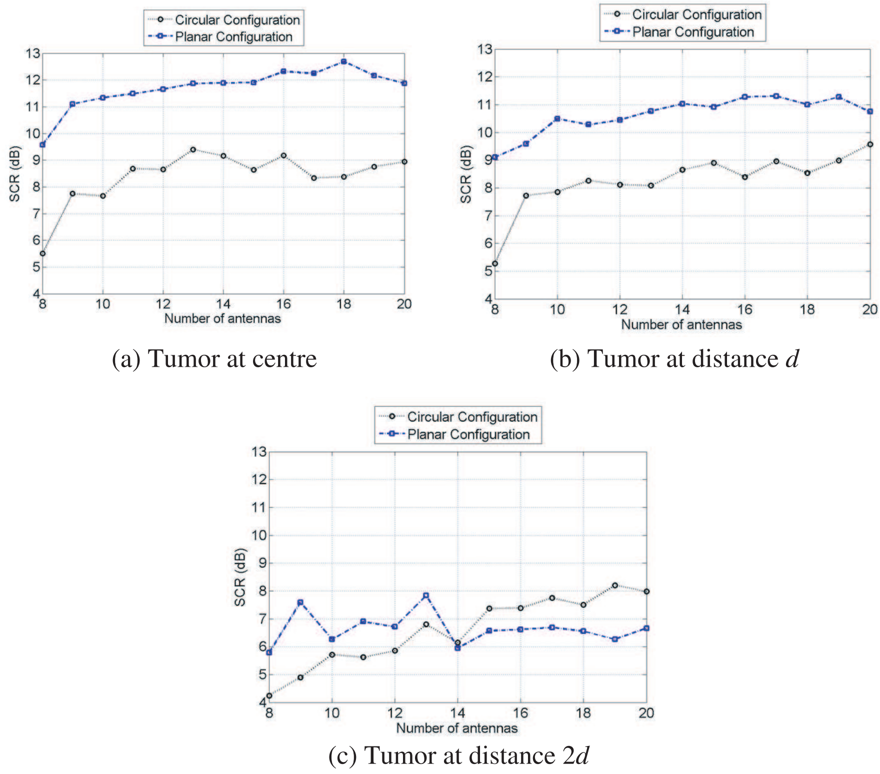

(a) Tumor at centre

(b) Tumor at distance d

(c) Tumor at distance $2d$

Figure 3. Variation of SCR with the number of antennas used for both planar and circular configurations.

the breast. The performance of the circular configuration is virtually independent of the tumor position. Conversely, the performance of the planar configuration tends to worsen when the distance of the tumor from the centre of the breast increases. This behaviour can be explained in terms of the average distances between the known tumor positions and the antennas for each configuration. When the average propagation distance increases, so too does the attenuation and phase effects of the channel, reducing the effectiveness of the beamformer. For the planar configuration, this average distance increases the further the tumor is from the centre of the breast, whereas for the circular configuration, this average distance does not show the same variation — this is logical since in the circular configuration if the tumor is further from one antenna, it necessarily means that it moves closer to another one.

Finally, very little improvement is noticed when the number of

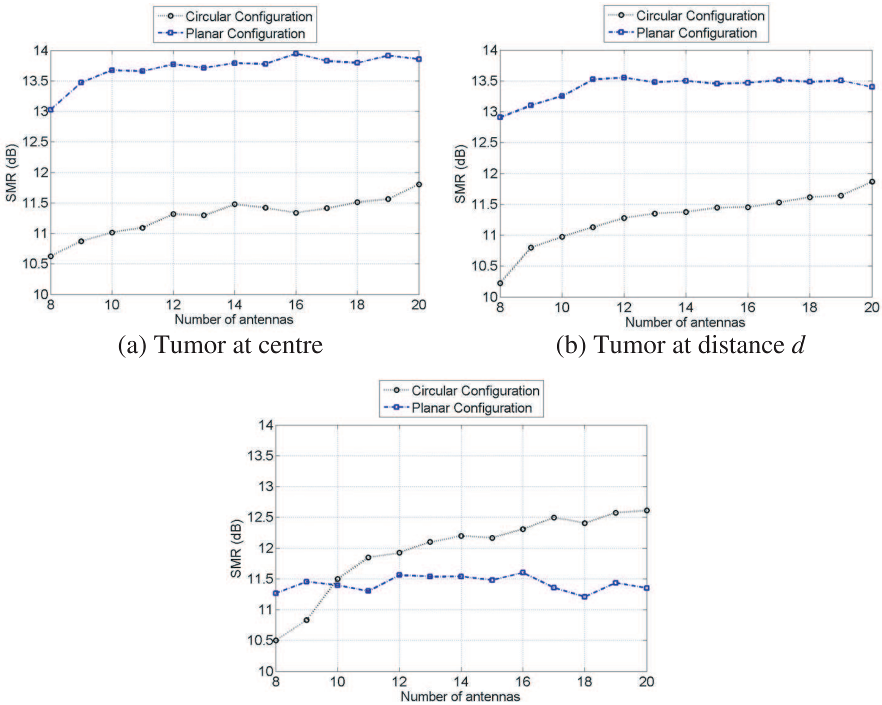

(a) Tumor at centre (b) Tumor at distance d

(c) Tumor at distance $2d$

Figure 4. Variation of SMR with the number of antennas used for both planar and circular configurations.

Table 2. Results for both antenna configurations with tumors located at three different distances from the centre of the breast, 0, d and $2d$, using 17 antennas.

Metric	Antenna Configuration	0	d	$2d$
SCR (dB)	Circular	8.34	8.96	7.76
	Planar	12.24	11.31	6.69
SMR (dB)	Circular	11.41	11.53	12.5
	Planar	13.83	13.51	11.36
M_{diff} (mm)	Circular	0.00	1.50	1.80
	Planar	2.69	2.92	4.95
FWHM (mm)	Circular	4.88	4.50	4.25
	Planar	8.00	8.00	9.00

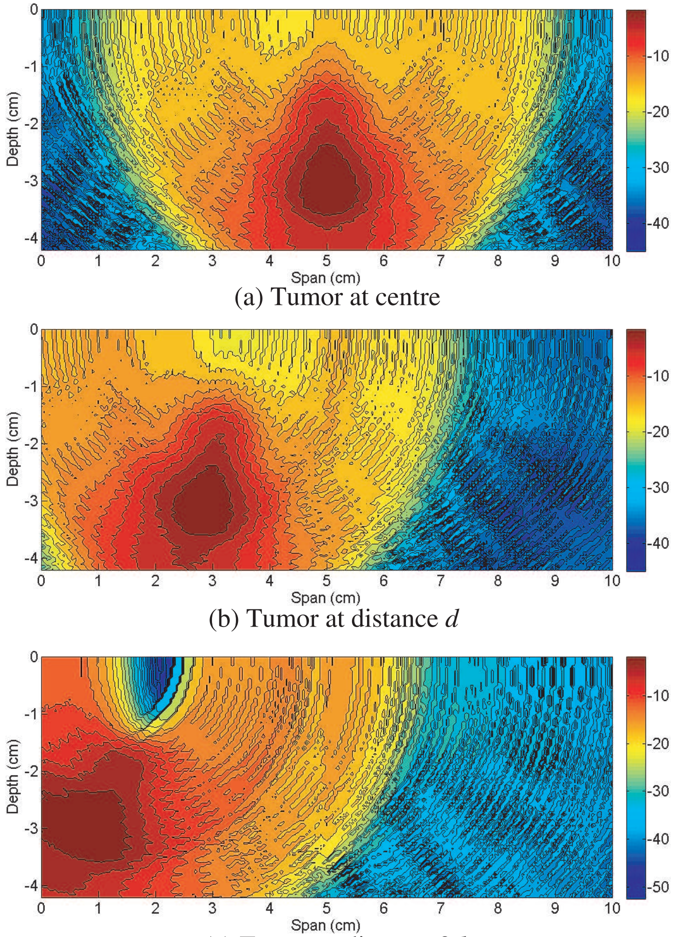

(a) Tumor at centre

(b) Tumor at distance d

(c) Tumor at distance $2d$

Figure 5. Images of backscattered energy (on a dB scale) for the planar antenna configuration using 17 antennas. A 6 mm tumor is centred at: (a) (−2.4, 5) cm, (b) (−2.4, 3) cm, (c) (−2.4, 1) cm.

antennas used exceeds 17, for both antenna configurations. Therefore, the optimized number of antennas used is 17. The resulting backscattered images (using 17 antennas) for the planar antenna configuration and the circular antenna configuration are shown in Figures 5 and 6, respectively.

From these figures, it is also evident that the circular configuration gives a clearer and more isolated position of the tumor when compared

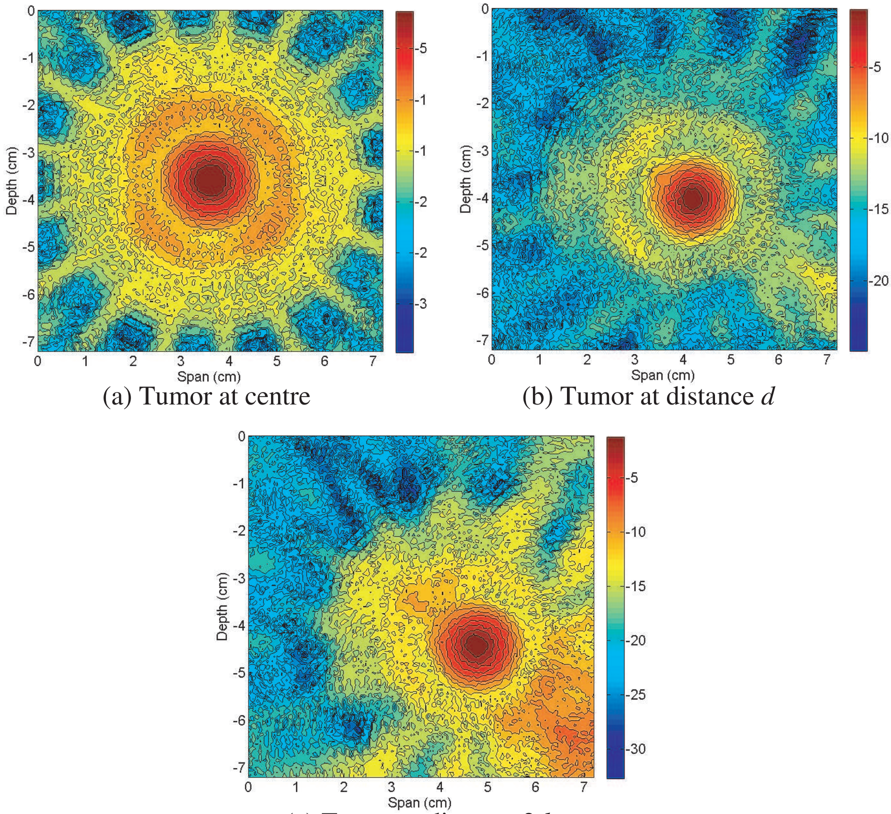

(a) Tumor at centre

(b) Tumor at distance d

(c) Tumor at distance $2d$

Figure 6. Images of backscattered energy (on a dB scale) for the circular antenna configuration using 17 antennas. A 6 mm tumor is centred at: (a) $(-3.6, 3.6)$ cm, (b) $(-3.95, 4.1)$ cm, (c) $(-4.3, 4.6)$ cm.

to its equivalent results for the planar configuration. This is also evident in the improved FWHM performance offered by the circular configuration, shown in Table 2. Also the centre of the tumor seems to be closer to its actual position for the circular configuration, as shown by the M_{diff} metric.

Using the planar configuration, the tumor appears closer to the skin than it actually is, suggesting that surrounding the breast with the antennas (in the circular configuration) provides for improved tumor localisation.

However, it is also evident that clutter is less significant in the planar images than in the circular images, which is consistent with the results for the SCR and the SMR presented in Figures 3 and 4,

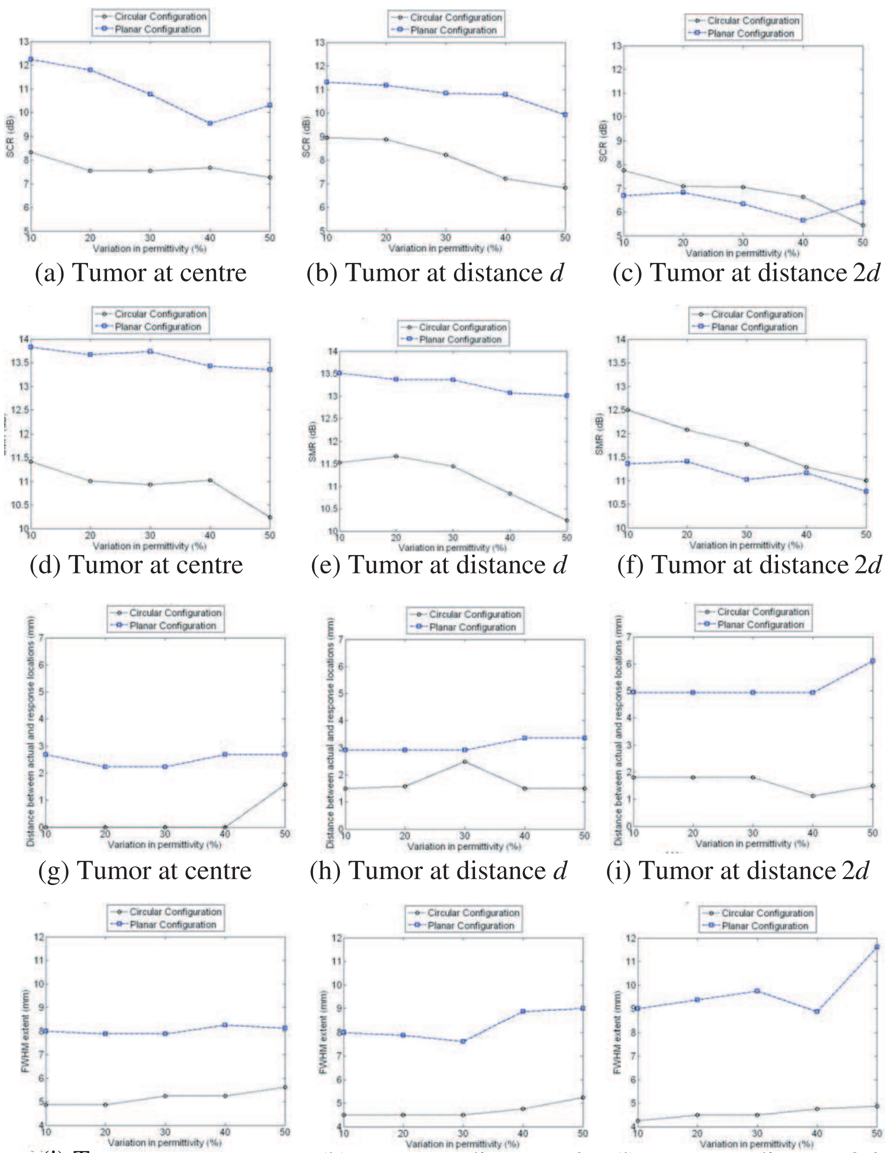

(a) Tumor at centre (b) Tumor at distance d (c) Tumor at distance $2d$

(d) Tumor at centre (e) Tumor at distance d (f) Tumor at distance $2d$

(g) Tumor at centre (h) Tumor at distance d (i) Tumor at distance $2d$

(j) Tumor at centre (k) Tumor at distance d (l) Tumor at distance $2d$

Figure 7. Effects of dielectric heterogeneity on both planar and circular antenna configuration. Each row corresponds to the metrics: SCR, SMR, M_{diff}, and FWHM. Each column corresponds to a tumor located at distance 0, d and $2d$ from the centre of the breast.

respectively. The planar configuration shows better performance in terms of both SCR and SMR, except for the $2d$ distance, as previously discussed. However, the circular configuration permits better localisation of the tumor, indicated by better Mdiff and FWHM results.

4.2. Effects of Increasing Dielectric Heterogeneity

In order to test the robustness of the two antenna configurations to greater variation in the dielectric properties of normal breast tissue, FDTD simulations are performed with increasing percentages of variation for permittivity and conductivity values of normal breast tissue, from ± 10 to $\pm 50\%$ in steps of 10%. These simulations all used the optimal number of 17 antennas for both configurations, derived from the first set of experiments.

Based on Figure 7, the SCR and the SMR show an overall decrease (with very few exceptions) with the increase of the dielectric variation, for both configurations. The tendency for the planar configuration to outperform the circular configuration when the distance between the tumor and the centre of the breast is 0 or d still holds with the variation in dielectric properties. Conversely, the circular configuration outperforms the planar configuration for the simulations in which the tumor is further from the centre of the breast when the dielectric variation increases.

Variations in M_{diff} occur with increasing dielectric variation, suggesting that this metric is relatively robust to dielectric variations for both configurations. Finally, examining the FWHM, which expresses the physical extent of the tumor response, the circular configuration exhibits very small variation with increasing heterogeneity. This highlights the localisation robustness of the circular system. With the planar configuration, the FWHM of the tumor response remains relaively constant when the tumor is centred in the breast; however, with the increase of the distance between the tumor and the breast centre, the planar system outputs higher values for this metric when the dielectric variation increases, thus reducing the localisation performance of the planar configuration.

5. CONCLUSIONS

This paper has examined the effect of antenna configuration on the performance of a UWB system for breast cancer detection. For test purposes, 2D FDTD models of the breast were created, with a tumor at various locations in the breast. Both planar and circular antenna configurations were tested through visual inspection and with four quantitative metrics: SCR, SMR, M_{diff} and FWHM. Seventeen antennas were chosen for both configurations, as it offered the best compromise of performance versus efficiency.

While the planar antenna configuration tended to outperform the circular configuration in terms of SCR and SMR when the tumor was located close to the centre of the breast, the circular antenna configuration outperformed the planar configuration at all other locations. Furthermore, the circular antenna configuration outperformed the planar configuration across the remaining metrics, suggesting that this configuration is much more effective in terms of tumor localisation.

Finally, the circular configuration was also shown to be more robust to natural variations in dielectric heterogeneity in terms of both M_{diff} and FWHM when compared to the planar-based system. The justification for the improved performance of the circular configuration is twofold: Firstly, the greater spatial distribution of the antennas around the entire breast in the circular configuration provides for improved tumor localization. Secondly, the shorter average propagation distance for signals recorded using the circular antenna configuration results in less attenuated reflections from the tumor. These relatively strong reflections are used to create improved images in terms of both SCR and SMR ratios. In conclusion, the circular configuration of antennas show much more consistent results in terms of tumor identification (SCR and SMR), independent of the location of the tumor location within the breast, and generally more precise tumor localization.

ACKNOWLEDGMENT

This work is supported by Science Foundation Ireland (SFI) under grant number 07/RFP/ENEF420.

REFERENCES

1. Society, A. C., "Cancer facts and figures 2008," *American Cancer Society*, 2008.
2. Nass, S. L., I. C. Henderson, and J. C. Lashof, *Mammography and Beyond: Developing Technologies for the Early Detection of Breast Cancer*, National Academy Press, 2001.
3. Elmore, J. G., M. B. Barton, V. M. Moceri, S. Polk, P. J. Arena, and S. W. Fletcher, "Ten-year risk of false positive screening

mammograms and clinical breast examinations," *New Eng. J. Med.*, Vol. 338, No. 16, 1089–1096, 1998.

4. Huynh, P. H., A. M. Jarolimek, and S. Daye, "The false-negative mammogram," *Radio Graphics*, Vol. 18, 1137–1154, 1998.
5. MacDonald, F. and C. H. J. Ford, *Molecular Biology of Cancer*, BIOS Scientific Publishers Limited, Oxford, 1997.
6. Hagness, S. C., A. Taflove, and J. E. Bridges, "Two-dimensional FDTD analysis of a pulsed microwave confocal system for breast cancer detection: Fixed-focus and antenna-array sensors," *IEEE Trans. Biomed. Eng.*, Vol. 45, No. 12, 1470–1479, 1998.
7. Bulyshev, A. E., S. Y. Semenov, A. E. Souvorov, R. H. Svenson, A. G. Nazorov, Y. E. Sizov, and G. P. Tatsis, "Computational modeling of three-dimensional microwave tomography of breast cancer," *IEEE Trans. Biomed. Eng.*, Vol. 48, No. 9, 1053–1056, Sep. 2001.
8. Meaney, P. M., M. W. Fanning, D. Li, S. P. Poplack, and K. D. Paulsen, "A clinical prototype for active microwave imaging of the breast," *IEEE Trans. Microwave Theory Tech.*, Vol. 48, No. 11, 1841–1853, Nov. 2000.
9. Meaney, P. M., K. D. Paulsen, J. T. Chang, M. W. Fanning, and A. Hartov, "Nonactive antenna compensation for fixed array microwave imaging Part II — Imaging results," *IEEE Trans. Med. Imag.*, Vol. 18, No. 6, 508–518, Jun. 1999.
10. Souvorov, A. E., A. E. Bulyshev, S. Y. Semenov, R. H. Svenson, and G. P. Tatsis, "Two dimensional analysis of a microwave flat antenna array for breast cancer tomography," *IEEE Trans. Microwave Theory Tech.*, Vol. 48, No. 8, 1413–1415, Aug. 2000.
11. Liu, Q. H., Z. Q. Zhang, T. Wang, J. A. Byran, G. A. Ybarra, L. W. Nolte, and W. T. Joines, "Active microwave imaging 1 — 2-D forward and inverse scattering methods," *IEEE Trans. Microwave Theory Tech.*, Vol. 50, No. 1, 123–133, Jan. 2002.
12. Meaney, P. M., M. W. Fanning, T. Raynolds, C. J. Fox, Q. Fang, C. A. Kogel, S. P. Poplack, and K. D. Paulsen, "Initial clinical experience with microwave breast imaging in women with normal Mammography," *Academic Radiology*, Vol. 14, No. 2, 207–218, 2007.
13. Kosmas, P. and C. M. Rappaport, "Time reversal with the FDTD method for microwave breast cancer detection," *IEEE Trans. Microwave Theory Tech.*, Vol. 53, No. 7, 2317–2323, Jul. 2005.
14. Kosmas, P. and C. M. Rappaport, "FDTD-based time reversal for microwave breast cancer detection-localization in three

dimensions," *IEEE Trans. Microwave Theory Tech.*, Vol. 54, No. 4, 1921–1927, Jun. 2006.

15. Hagness, S. C., A. Taflove, and J. E. Brdiges, "Three-dimensional FDTD analysis of a pulsed microwave confocal system for breast cancer detection: Design of an antenna array element," *IEEE Trans. Antennas and Propagat.*, Vol. 47, 783–791, May 1999.
16. Fear, E. C., X. Li, S. C. Hagness, and M. A. Stuchly, "Confocal microwave imaging for breast cancer detection: Localization of tumors in three dimensions," *IEEE Trans. Biomed. Eng.*, Vol. 49, No. 8, 812–812, 2002.
17. Fear, E. C. and M. A. Stuchly, "Microwave system for breast tumor detection," *IEEE Microwave and Guided Wave Letters*, Vol. 9, No. 11, 470–472, Nov. 1999.
18. Fear, E. C., J. Sill, and M. A. Stuchly, "Experimental feasibility study of confocal microwave imaging for breast tumor detection," *IEEE Trans. Microwave Theory Tech.*, Vol. 51, No. 3, 887–892, Mar. 2003.
19. Fear, E., J. Sill, and M. Stuchly, "Microwave system for breast tumor detection: experimental concept evaluation," *IEEE AP-S International Symposium and USNC/URSI Radio Science Meeting*, Vol. 1, 819–822, San Antonio, Texas, Jun. 2002.
20. Li, X. and S. C. Hagness, "A confocal microwave imaging algorithm for breast cancer detection," *IEEE Microwave and Wireless Components Letters*, Vol. 11, No. 3, 130–132, 2001.
21. Li, X., E. J. Bond, B. D. V. Veen, and S. Hagness, "An overview of ultra-wideband microwave imaging via space-time beamforming for early-stage breast-cancer detection," *IEEE Antennas and Propagation Magazine*, Vol. 47, No. 1, 19–34, Feb. 2005.
22. Craddock, I. J., R. Nilavalan, J. Leendertz, A. Preece, and R. Benjamin, "Experimental investigation of real aperture synthetically organised radar for breast cancer detection," *IEEE AP-S Inter. Sym.*, Vol. 1B, 179–182, Washington, DC, 2005.
23. Hernandez-Lopez, M., M. Quintillan-Gonzalez, S. Garcia, A. Bretones, and R. Martin, "A rotating array of antennas for confocal microwave breast imaging," *Microw. Opt. Technol. Lett.*, Vol. 39, No. 4, 307–311, 2003.
24. De Rodriguez, M. E., M. Vera-Isasa, and V. Del Rio, "3-D-microwave breast tumor detection: Study of system performance," *IEEE Trans. Biomedical Eng.*, Vol. 55, No. 12, 2772–2777, Dec. 2008.
25. Davis, S. K., E. J. Bond, X. Li, S. C. Hagness, and B. D. Van-Veen,

"Microwave imaging via space-time beamforming for the early detection of breast cancer: Beamformer design in the frequency domain," *Journal of Electromagnetic Waves and Applications*, Vol. 17, No. 2, 357–381, 2003.
26. Bond, E. J., X. Li, S. C. Hagness, and B. D. V. Veen, "Microwave imaging via space-time beamforming for early detection of breast cancer," *IEEE Trans. Antennas and Propagat.*, Vol. 51, No. 8, 1690–1705, Aug. 2003.
27. Joines, W., Y. Zhang, C. Li, and R. L. Jirtle, "The measured electrical properties of normal and malignant human tissues from 50 to 900 MHz," *Med. Phys.*, Vol. 21, 547–550, 1993.
28. Sha, L., E. R. Ward, and B. Stroy, "A review of the dielectric properties of normal and malignant breast tissue," *Proceedings of the IEEE SoutheastCon*, 457–462, Columbia, South Carolina, USA, Apr. 2002.
29. Surowiec, A. J., S. S. Stuchly, J. R. Barr, and A. Swarup, "Dielectric properties of breast carcinoma and the surrounding tissues," *IEEE Trans. Biomed. Eng.*, Vol. 35, No. 4, 257–263, 1988.
30. Campbell, A. M. and D. V. Land, "Dielectric properties of female human breast tissue measured in vitro at 3.2 GHz," *Phys. Med. Biol.*, Vol. 37, No. 1 193–210, 1992.
31. Lazebnik, M., D. Popovic, L. McCartney, C. B. Watkins, M. J. Lindstrom, J. Harter, S. Sewall, T. Ogilvie, A. Magliocco, T. M. Breslin, W. Temple, D. Mew, J. H. Booske, M. Okoniewski, and S. C. Hagness, "A large-scale study of the ultrawideband microwave dielectric properties of normal, benign and malignant breast tissues obtained from cancer surgeries," *Phys. Med. Biol.*, Vol. 52, 6093–6115, 2007.
32. Lazebnik, M., L. McCartney, D. Popovic, C. B. Watkins, M. J. Lindstrom, J. Harter, S. Sewall, A. Magliocco, J. H. Booske, M. Okoniewski, and S. C. Hagness, "A large-scale study of the ultrawideband microwave dielectric properties of normal breast tissue obtained from reduction surgeries," *Phys. Med. Biol.*, Vol. 52, 2637–2656, 2007.
33. Hagness, S. C., A. Taflove, M. Popovic, and J. E. Bridges, *Microwave Discrimination between Malignant and Benign Breast Tumors*, Patent: 6421550, L. L. C. Interstitial, 2002.
34. Joines, W. T., "Frequency-dependent absorption of electromagnetic energy in biological tissue," *IEEE Trans. Biomedical Eng.*, Vol. 31, No. 1, 17–20, 1984.
35. Pethig, R., "Dielectric properties of biological materials: biophysical and medical applications," *IEEE Transactions on*

Electrical Insulation, Vol. E1–E19, No. 5, 453–474, 1984.
36. Chaudhary, S. S., R. K. Mishra, A. Swarup, and J. M. Thomas, "Dielectric properties of normal and malignant human breast tissue at radiowave and microwave frequencies," *Indian J. Biochem. Biophys.*, Vol. 21, 76–79, 1984.
37. Nilavalan, R., A. Gbedemah, X. Li, and S. C. Hagness, "Numerical investigation of breast tumour detection using multi-static radar," *IET Electronic Letters*, Vol. 39, No. 25, 1787–1789, Dec. 2003.
38. O'Halloran, M., M. Glavin, and E. Jones, "Quasi-multistatic MIST beamforming for the early detection of breast cancer," *IEEE Trans. Biomedical Eng.*, in press.
39. Fear, E. C. and M. A. Stuchly, "Microwave detection of breast cancer," *IEEE Trans. Microwave Theory Tech.*, Vol. 48, No. 11, 1854–1863, Nov. 2000.
40. Xie, Y., B. Guo, L. Xu, J. Li, and P. Stoica, "Multistatic adaptive microwave imaging for early breast cancer detection," *IEEE Trans. Biomedical Eng.*, Vol. 53, No. 8, 1647–1657, 2006.
41. Klemm, M., I. J. Craddock, J. A. Leendertz, A. Preece, and R. Benjamin, "Improved delay-and-sum beamforming algorithm for breast cancer detection," *International Journal of Antennas and Propagation*, Vol. 2008, 2008.
42. Fear, E. C. and M. Okoniewski, "Confocal microwave imaging for breast tumor detection: Application to a hemispherical breast model," *Microwave Symposium Digest, 2002 IEEE MTT-S International*, Vol. 3, 1759–1762, Seattle, WA, USA, 2002.
43. Xie, Y., B. Guo, J. Li, and P. Stoica, "Novel multistatic adaptive microwave imaging methods for early breast cancer detection," *EURASIP J. Appl. Si. P.*, Vol. 2006, No. Article ID: 91961, 1–13, 2006.
44. Klemm, M., I. J. Craddock, J. Leendertz, A. W. Preece, and R. Benjamin, "Breast cancer detection using symmetrical antenna array," *Proceedings of the 2nd European Conference on Antennas and Propagation (EuCAP'07)*, 1–5, Edinburgh, UK, Nov. 2007.
45. Craddock, I. J., M. Klemm, J. Leendertz, A. W. Preece, and R. Benjamin, "Development and application of a UWB radar system for breast imaging," *Antennas and Propagation Conference, 2008. LAPC 2008. Loughborough*, 24–27, 2008.
46. Conceição, R. C., M. O'Halloran, M. Glavin, and E. Jones, "Antenna configurations for ultra wide band radar detection of breast cancer," *SPIE BIOS West*, Vol. 7169, San Jose, CA, Jan. 2009.

47. Gabriel, C. and S. Gabriel. (Last accessed: Sept. 2009) Compilation of the Dielectric Properties of Body Tissues at RF and Microwave Frequencies. [Online]. Available: http://niremf.ifac.cnr.it/tissprop/.
48. Lim, H. B., N. T. T. Nhung, E. P. Li, and N. D. Thang, "Confocal microwave imaging for breast cancer detection: Delay-multiplyand-sum image reconstruction algorithm," *IEEE Trans. Biomedical Eng.,* Vol. 55, No. 6, 1697–1704, June 2008.